


Compressive strain engineering of strong and sensitive pseudomagnetic fields in buckled graphene nanobubbles

Xiaoyi Yuan  and Shuze Zhu ^{*}

Center for X-Mechanics, Key Laboratory of Soft Machines and Smart Devices of Zhejiang Province, Department of Engineering Mechanics, Institute of Applied Mechanics, School of Aeronautics and Astronautics, Zhejiang University, Hangzhou 310000, China

 (Received 17 December 2022; revised 23 February 2023; accepted 17 April 2023; published 9 May 2023)

The formation of pseudomagnetic fields is a well-known consequence due to lattice strain, which has considerable effects on the electronic properties of graphene. To this end, strain engineering remains an effective route to enable unconventional electronic properties. Particularly, pseudomagnetic fields due to compressive strain have demonstrated unique advantages such as remarkably high intensities at relatively low magnitude of strains (e.g., $< 5\%$) in several experiments. For example, pseudomagnetic fields as high as 300 T have been observed in buckled graphene nanobubbles. Recently, strong pseudomagnetic fields as high as 108 T have been measured in periodically buckled monolayer graphene, responsible for its band flattening and correlated states. Nevertheless, the general features and sensitivities of compressive strain-induced pseudomagnetic fields have been rarely explored, posing challenges for realizing their full potential. In this paper, we carry out large-scale molecular dynamics simulations to explore the properties of pseudomagnetic fields in buckled graphene nanobubbles, which are the basic representative graphene structures under compressive strains. We reveal that compressive strain can induce strong and sensitive pseudomagnetic fields for a variety of nanobubble shapes and boundary relaxation conditions. We also discuss the effect of the microscopy probe tip, which is frequently used to tune the morphologies and strain patterns. These results may offer guidance for designing electronic two-dimensional structures enabled by compressive strain engineering.

DOI: [10.1103/PhysRevB.107.195417](https://doi.org/10.1103/PhysRevB.107.195417)

I. INTRODUCTION

The formation of pseudomagnetic fields is a well-known consequence due to lattice strain, which has considerable effects on the electronic properties of graphene [1,2]. Recently, the periodical pseudomagnetic fields have been shown to induce flat band dispersion in buckled monolayer graphene [3], which could potentially offer an alternative platform to study correlated states other than twisted bilayer graphene. Controlling the pseudomagnetic field of graphene through strain engineering is thus crucial for enabling unconventional electronic properties. Over the years, tremendous attention has been paid to manipulating the strain field in graphene. Both triaxial [4] and uniaxial tensile loading [5] of patterned graphene have demonstrated the capacity to achieve quasiuniform pseudomagnetic fields with large intensities. The microscopy probe tip has also been frequently used not only to measure the electronic states [2] but also to induce localized strain field or morphological change by taking advantage of the interaction between the probe tip and graphene. For example, the localized deformation induced by the scanning tunneling microscopy (STM) probe tip creates threefold symmetry pseudomagnetic fields, the distribution of which allows the confinement of electrons like the effect of a quantum dot [6]. Another recent example is the programmable formation of graphene nanobubbles and threefold symmetry pseudomag-

netic fields with the help of the atomic force microscope tip [7]. There are also investigations on the pseudomagnetic fields in a graphene nanobubble inflated with gas molecules [8].

Typical strain engineering considerations are based on tensile deformation [4–8] (e.g., a graphene nanobubble inflated with gas molecules [8], triaxial tensile loading [4], uniaxial tensile loading [5]). Compressive strain engineering, on the other hand, remains an alternative route and has several impressive demonstrations. For example, the pseudomagnetic field in buckled graphene nanobubbles can reach as high as 300 T [2], while the strain is estimated to be $\sim 4\%$. Very recently, remarkable experimental evidence on strong pseudomagnetic field as high as 108 T from periodically buckled monolayer graphene hints at another possibility for accessing correlated electronic states other than magic-angle twist bilayer graphene [3,9], although the magnitude of compressive strains can be $< 5\%$ [3]. This experimental evidence suggests that compressive strain engineering can potentially offer a much higher intensity of pseudomagnetic field than that of tensile strain engineering and thus much stronger effects on the dynamics of electrons. Nevertheless, most available theoretical and computational investigations are mainly focused on tensile strain engineering; the general features and the sensitivity of the pseudomagnetic field due to compressive strain engineering have been rarely explored, posing challenges for realizing its full potential.

To address the above issues, in this paper, we systematically investigate buckled graphene nanobubbles, which are basic representative structural forms of graphene under

^{*}Corresponding author: shuzezhu@zju.edu.cn

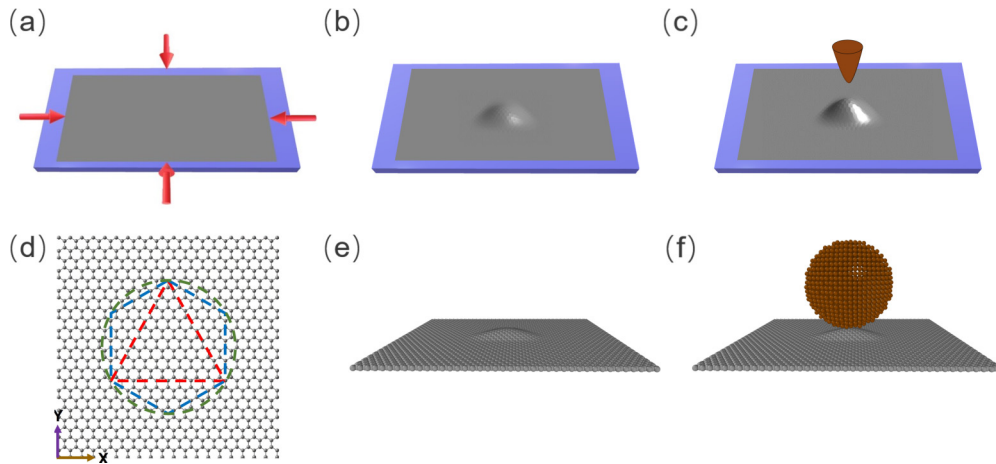


FIG. 1. (a) Schematic of monolayer graphene (gray) on substrate (purple) under in-plane compression (red arrows). (b) Schematic of the buckled nanobubble structure. (c) Schematic of the buckled nanobubble structure interacting with the probe tip (brown cone). (d) Schematic showing three shapes of boundaries (triangular, hexagonal, and circular, marked by dashed lines) of nanobubbles. The atoms inside the boundaries are free to move, while those outside the boundaries are fixed. (e) Illustration of atomic structure of the buckled nanobubble without the probe tip. We employ a virtual substrate to support graphene. (f) Illustration of atomic structure of the buckled nanobubble interacted with a probe tip, which is modeled as a sphere.

compressive strain. The graphene nanobubble study in this paper is generated by buckling, which is induced by in-plane compression. Using large-scale molecular dynamics (MD) simulations, we reveal how the pseudomagnetic field is affected by the geometry of the nanobubbles, the applied global compressive strain, and the presence of the external microscopic probe tip. Particularly, we find that the intensity of the pseudomagnetic field can be high and very sensitive to perturbation from strain field. Our study is expected to deepen the understanding of pseudomagnetic field of graphene in terms of compressive strain engineering.

II. COMPUTATIONAL MODELS AND METHODS

In this paper, we aim to reveal how the globally applied in-plane uniform compressive strain and the interaction with an external microscopic probe tip affect the pseudomagnetic fields in buckled graphene nanobubbles of various shapes and sizes. Specifically, the magnitude of compressive strain that induced the buckling, the radius of the microscopic probe tip, the shapes of nanobubbles (i.e., triangular, hexagonal, and circular), and the nanobubble boundary conditions (i.e., fixed boundary and relaxed boundary) are the influencing factors under consideration in this paper.

Since the buckling problem due to compressive strain concerns large deformation and is highly nonlinear and the interactions with the probe tip are long-range van der Waals forces, developing a continuum mechanics analytical theory is not a straightforward task. Considering the scope of this paper, we resort to MD simulations, which are performed with LAMMPS [10]. In this paper, we are concerned with a graphene nanobubble due to the in-plane compression-induced buckling [Figs. 1(a) and 1(b)]. Initially, a flat graphene monolayer is deposited on a substrate [Fig. 1(a)]. Then a displacement field of uniform biaxial shrinking [indicated by the red arrows in Fig. 1(a)] is applied to graphene to induce compressive strain. In principle, a large in-plane shrinking

displacement field could induce the formation of buckled nanobubbles [Fig. 1(b)]. Experimentally, the compressive strain field could be introduced using a prestretched flexible substrate [11], due to the difference in thermal expansion coefficient [2], or due to the lattice mismatch [12]. We choose to investigate circular, hexagonal, and triangular nanobubbles because these simple shapes may be suitable for experimental exploration.

The microscopy probe tip [Fig. 1(c)] has been frequently used not only in characterizing the electronic states but also as an effective tool to engineer the morphologies and strain patterns in two-dimensional materials [13,14]. To this end, how the probe tip affects the intrinsic pseudomagnetic field in buckled graphene structures is an intriguing question that has been subjected to investigation in this paper. In our MD simulation, we simulate a STM probe tip composed of Pt atoms. The shape of the tip is a sphere [Fig. 1(f)] with an assigned radius. The simulation of the effect of the probe tip follows the strategy outlined in earlier works [6,15]. The probe tip is initially placed directly above the nanobubble and then gradually moves away from the nanobubble along the vertical direction. Due to the interaction between the tip and the nanobubble, the height of the nanobubble would gradually increase to its critical value, after which the tip loses contact with the nanobubble. We investigate the out-of-plane deflection of the nanobubble at the critical state where the contact between the probe tip and the nanobubble is minimum. In this paper, the tip size refers to the radius of the probe tip.

Both fixed and relaxed boundary conditions are considered. For fixed boundaries with triangular, hexagonal, and circular shapes [Fig. 1(d)], the atoms outside the boundary are not allowed to relax after the application of the shrinking displacement field, while those atoms inside the boundary are free to adjust their positions in response to the compressive strain field. As a result, beyond a certain amount of applied compressive strain, the graphene buckles into a nanobubble.

For the relaxed boundary condition, some atoms outside the boundary are allowed to move but are subjected to constraints which limit their maximum displacement (more details are discussed in related sections). In this paper, the nanobubble size is defined as the diameter of the circular fixed boundary or the diameter of the circumscribed circle of triangular and hexagonal fixed boundaries.

In all simulations, the zigzag direction of graphene is aligned with the x direction [Fig. 1(d)]. We use the AIREBO potential to describe the C-C interactions inside graphene [16]. The Lennard-Jones 9-3 potential is chosen for the interaction between the graphene and the virtual substrate:

$$V(r) = \epsilon \left[\frac{2}{15} \left(\frac{\sigma}{r} \right)^9 - \left(\frac{\sigma}{r} \right)^3 \right]. \quad (1)$$

Here, ϵ (energy unit) and σ (distance unit) are two parameters of the potential, while r is the vertical distance between the carbon and the virtual substrate plane. The virtual substrate is located in the equilibrium position directly below the graphene. In this paper, we are more focused on the buckling-induced intrinsic pseudomagnetic field at the interior of the nanobubble so that we use a parameter set ($\epsilon = 0.00001$ eV, $\sigma = 2.9943$ Å) that minimizes the effect of substrate interaction. Stronger substrate interaction usually only influences the region close to the nanobubble boundary vertex (see Appendix A). It is expected that stronger substrate interaction would effectively tighten the constraints from the boundaries. Future work may be needed to systematically investigate the effect of substrate interaction. The interatomic pair interaction between platinum and carbon atoms is modeled using the conventional Lennard-Jones 12-6 potential with $\epsilon_{\text{C-Pt}} = 0.0039744$ eV, $\sigma_{\text{C-Pt}} = 2.9422$ Å. The parameters are determined through the customary Lorentz-Berthelot mixing rules, using the platinum-platinum and carbon-carbon parameters [17]. After the application of global in-plane compressive strain, the graphene membrane is first relaxed for 10 ps to allow the formation of a buckled nanobubble structure if the compressive strain is large enough. Then the energy of the system is minimized to obtain the optimized nanobubble structure. The canonical (NVT) ensemble is used for the dynamics run in the relaxation stage, and a Nosé-Hoover thermostat is used to maintain the temperature at 5 K (see Appendix B for a discussion of the effect of temperature). Note that the typical temperature for STM measurement is < 5 K. The energy minimization uses the Hessian-free truncated Newton algorithm until the total energy change between successive iterations divided by the energy magnitude is $\leq 10^{-10}$. From the optimized structure, the atomistic displacement field of the nanobubble can be obtained, from which the pseudomagnetic field can be calculated, as explained below.

In continuum mechanics, the strain tensor is written in Cartesian material coordinates (X_i) as [8]

$$u_{ij} = \frac{1}{2} \left(\frac{\partial u_i}{\partial X_j} + \frac{\partial u_j}{\partial X_i} \right) + \frac{1}{2} \left(\frac{\partial u_k}{\partial X_i} \frac{\partial u_k}{\partial X_j} \right). \quad (2)$$

The displacement of each atom can be obtained by comparing the initial and final coordinates of each atom. Then by numerical interpolation, a continuum displacement field for the entire surface of the nanobubble is obtained. The

strain field can then be obtained by finding the gradient of the displacement components according to Eq. (2). The lattice distortions due to strain in graphene introduce effective gauge field \mathbf{A}_{ps} in the Dirac Hamiltonian [18], leading to a pseudomagnetic field \mathbf{B}_{ps} . The strain-induced pseudogauge field \mathbf{A}_{ps} is calculated from the strain components u_{ij} as [6,19]

$$\mathbf{A}_{ps} = \frac{t\beta}{ev_F} (u_{xx} - u_{yy}, -2u_{xy}), \quad (3)$$

where $\beta = 2.5$ is the dimensionless constant, $t = 2.8$ eV is the hopping energy, and $v_F = 1 \times 10^6$ ms $^{-1}$ is the Fermi velocity. Then the pseudomagnetic field can be calculated as $\mathbf{B}_{ps} = \nabla \times \mathbf{A}_{ps}$, which may be nonzero along the z direction. The field value can be calculated as

$$B_{ps} = \frac{t\beta}{ev_F} \left[\frac{\partial(-2u_{xy})}{\partial x} - \frac{\partial(u_{xx} - u_{yy})}{\partial y} \right]. \quad (4)$$

In this paper, the field intensity refers to the absolute value of the field value, unless otherwise notified.

III. RESULT AND DISCUSSION

A. Intrinsic pseudomagnetic fields

We start our atomistic simulations on a representative system that has been explored experimentally [2], where the triangular nanobubble possesses a pseudomagnetic field as high as 300 T. Although the strain fields and the resulting pseudomagnetic fields have been analyzed by using a triangular lattice [20] to model graphene [2], here, we provide insights directly from atomistic simulations. In accordance with experimental characterization [2], the triangular nanobubble size in our model is 4.7 nm [Fig. 2(a)], where the gray lines denote the boundary of the triangular nanobubble. The applied global uniform in-plane compressive strain to trigger the buckling is set to 0.035. Figure 2(a) shows the out-of-plane deformed morphology of the buckled nanobubble induced by the compressive strain. The deformation has an axisymmetric tentlike shape. The height of the nanobubble is ~ 0.3 nm. Figures 2(b)–2(d) show the contour plots of the components of the Lagrange strain tensor in the nanobubble. For visual clarity, the strain field outside the boundary is not shown (such a procedure is enforced for all figures until otherwise notified). The normal strain components (u_{xx} and u_{yy}) are negative due to the nature of buckling. The magnitude of the normal strain near the fixed boundary is in general larger than that in the central region. The shear strain can be positive or negative depending on the location. The magnitude of the shear strain also diminishes at the central region. Figures 2(e) and 2(f) plot the resulting pseudomagnetic field in the triangular nanobubble. A relatively uniform strain-induced pseudomagnetic field of ~ 300 T across the central region can be seen. There are also strong pseudomagnetic fields localized near the boundary (including near the vertices). The strong pseudomagnetic fields in the central region and near the boundary would act to confine the motion of electrons. The deformation profile of the nanobubble and the intensity profile of the pseudomagnetic field explain the experimental results well [2], validating our computational methods.

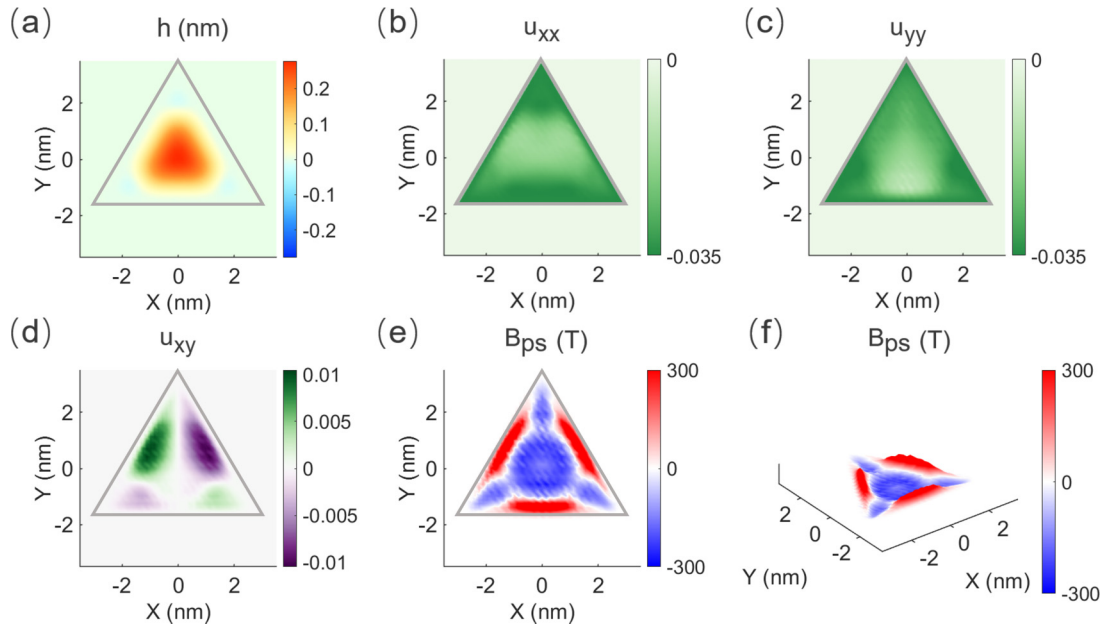


FIG. 2. Simulation results for a representative buckled triangular nanobubble. The gray lines represent nanobubble boundaries. The triangular nanobubble size is 4.7 nm. The applied global uniform in-plane compressive strain to trigger the buckling is 0.035. (a) Out-of-plane deflection (h). (b)–(d) Strain components u_{xx} , u_{yy} , and u_{xy} , respectively. (e) Top view of the pseudomagnetic field (B_{ps}). (f) Perspective view of the pseudomagnetic field. These results agree with experimental measurement, validating our computational methods.

Next, we discuss the effect of the nanobubble shapes (Fig. 3). For illustration, the nanobubble size for three shapes (triangular, hexagonal, and circular) of nanobubbles is uniformly set to 4.7 nm, and the applied global in-plane compressive strain is set to 0.03. Figure 3(a) is the result for

the triangular nanobubble. Although the applied compressive strain only reduces by 0.005 compared with the case shown in Fig. 2, the maximum pseudomagnetic field intensity in the central region is reduced drastically to ~ 150 T. This is the first hint of the sensitivity of the pseudomagnetic field in buckled

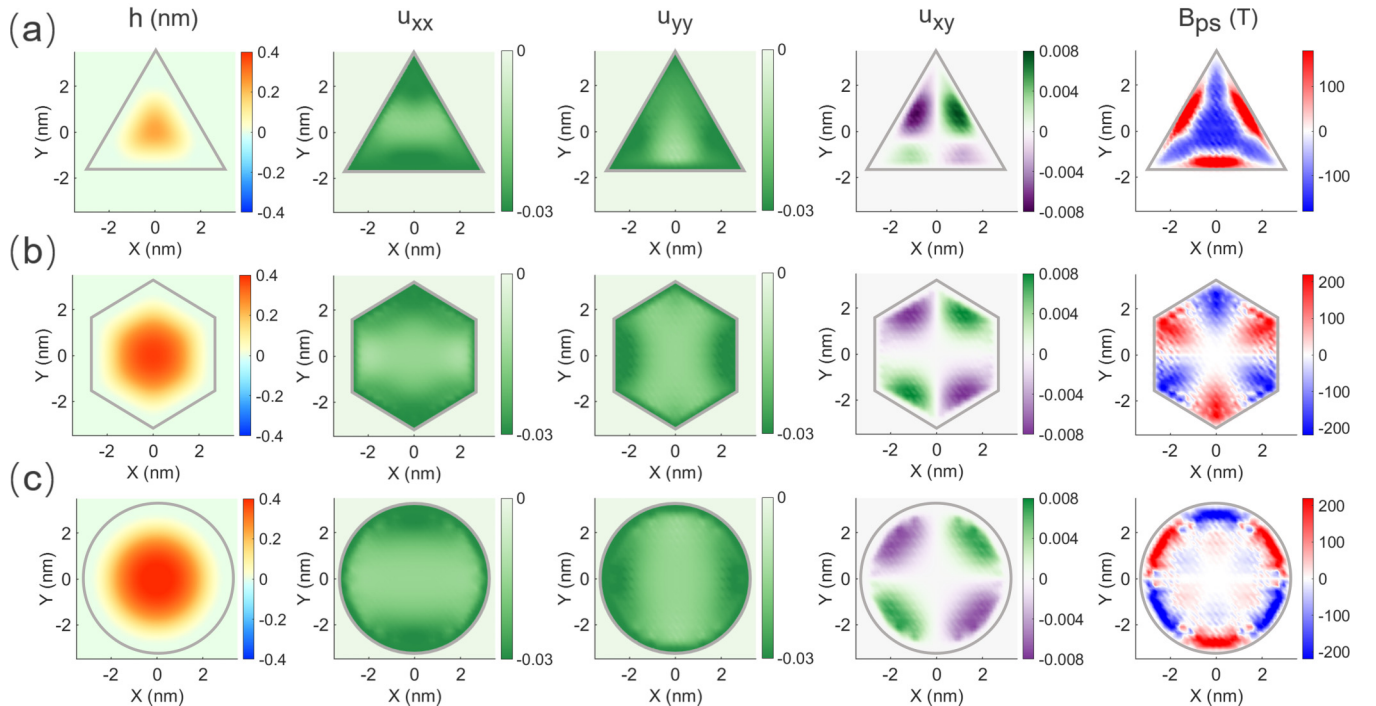


FIG. 3. Shape-dependent simulation results for representative buckled nanobubbles of three shapes, showing out-of-plane deflection (h), strain components (u_{xx} , u_{yy} , and u_{xy}), and the pseudomagnetic field (B_{ps}). The gray lines represent nanobubble boundaries of (a) triangular, (b) hexagonal, and (c) circular shape. In all cases, the nanobubble sizes are 4.7 nm, and the applied compressive strains are 0.03.

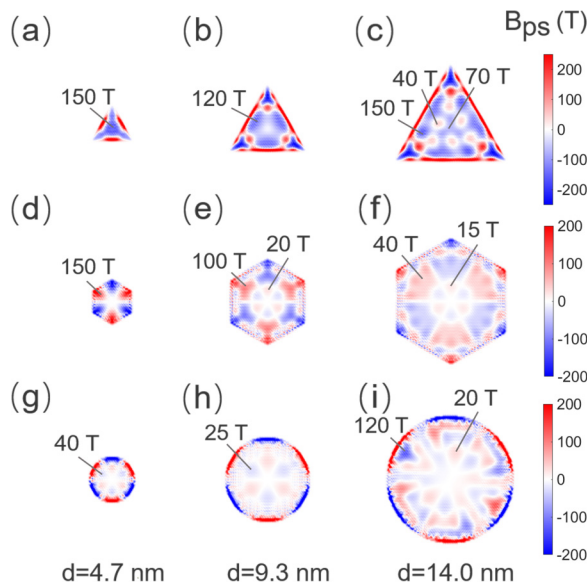


FIG. 4. Pseudomagnetic fields for nanobubbles of three shapes and different sizes: (a) triangular, (b) hexagonal, and (c) circular. The nanobubble sizes are 4.7, 9.3, and 14.0 nm, respectively. For all cases, the applied compressive strains are 0.03. Generally, increasing the nanobubble size complicates the field distribution patterns while decreasing the interior pseudomagnetic field intensity.

graphene nanobubble with respect to the applied compressive strain.

For hexagonal nanobubbles of the same size [Fig. 3(b)], the distribution of the out-of-plane deflection and strain components roughly follows the pattern as in triangular nanobubbles [Fig. 3(a)]. Unlike the triangular nanobubble, the pseudomagnetic field intensity is almost zero at the central region. The high-intensity fields with alternating signs are located at the regions near the six vertices; together they represent a threefold symmetry. The field intensity of the region near the six vertices reaches ~ 150 T. For circular nanobubbles of the same size [Fig. 3(c)], the pseudomagnetic field intensity at the interior region further reduces. The maximum intensity of the pseudomagnetic field (~ 200 T) is observed near the circular boundary. At the interior region of the nanobubble, we can still observe a threefold symmetry pseudomagnetic field, with the maximum field intensity of ~ 30 T. Briefly, a buckled nanobubble of higher symmetry shape suppresses the field intensity at the interior region while enhancing the field intensity close to the boundary. Pseudomagnetic fields always have threefold symmetry because the applied compressive strain is axisymmetric.

Then we proceed to the discussion of the effect of the nanobubble sizes. Figures 4(a)–4(c) plot the pseudomagnetic field in triangular nanobubbles with sizes of 4.7, 9.3, and 14.0 nm, respectively. Same as in Fig. 3, the applied compressive strains are 0.03. It is observed that, as the triangular nanobubble size increases, the pseudomagnetic field at the interior region no longer appears to be uniform, although it is still technically under triaxial loading [4]. Here, we see that triaxial compressive loading does not always generate a uniform distribution of pseudomagnetic fields, which can be distinct from the tensile triaxial loading case [4]. The characteristic

observation is that an increasing number of embedding regions with opposite signs of the pseudomagnetic field appears as the nanobubble size increases [Figs. 4(b) and 4(c)]. For example, in Fig. 4(c), the positive and negative pseudomagnetic field intensities are 70 and 40 T, respectively. The field intensity at the interior regions decreases as the nanobubble size increases, although the applied compressive strains are kept the same. The field intensities are still high at the regions near the boundary lines and the vertices due to large strain gradients near the location of strong spatial constraints. For hexagonal and circular shapes, the increase in bubble size appears to have even more complex effects. For the smallest size model as shown in Fig. 4(d), three narrow linelike regions with zero field intensity passing through the center demarcate the hexagon into six regions with nontrivial field intensity (~ 150 T), arranging themselves in a pattern of threefold symmetry. As the hexagonal nanobubble size doubles, a ring region with zero field intensity emerges, surrounding the center of the hexagon [Fig. 4(e)]. Together with the three linelike regions, they demarcate the hexagon into multiple regions, where neighboring regions carry opposite signs. The overall field intensities at the interior regions also decrease, while the field intensities are still the highest at regions close to the boundary. As the hexagonal bubble size further increases [~ 3 times the size in Fig. 4(d)], the distribution pattern near the vertices becomes even more complicated [Fig. 4(f)], while the overall field intensities further decrease. The results from the circular shaped buckled nanobubble [Figs. 4(g)–4(i)] also exhibit a similar trend. The increase in the nanobubble size complicates the field distribution patterns while decreasing the interior pseudomagnetic field intensity.

It is important to realize that the pseudomagnetic fields in buckled nanobubbles due to compressive strain are fundamentally different than those in pressurized nanobubbles due to tensile strain [8]. First, for pressurized nanobubbles [8], except in highly anisotropic geometries, the pseudomagnetic field is generally significant only near the nanobubble boundaries. The reason is that, under gas pressure, the interior region of the nanobubble displays nearly isotropic strain, which has almost zero strain gradient, leading to almost zero pseudomagnetic field [8]. Nevertheless, in the buckled nanobubbles, the interior region of the bubble can still have very strong pseudomagnetic fields because the strain is anisotropic due to buckling instability. Second, for pressurized triangular nanobubbles [8], the pseudomagnetic field at the interior region would always be uniform due to the triaxial tensile loading state [4]. Nevertheless, nonuniform pseudomagnetic fields can be found at the interior region of the buckled triangular nanobubble under triaxial compressive loading [Fig. 4(c)]. This is caused by the anisotropic strain gradient due to buckling instability. Third, high pressure is needed to achieve strong intensity of pseudomagnetic fields in pressurized nanobubbles [8]. Nevertheless, strong pseudomagnetic fields in buckled nanobubbles can be achieved for only a small amount of compressive strain.

Then we carry out large-scale MD studies to investigate the averaged intensity of the pseudomagnetic fields at the interior regions of three shapes of nanobubbles as a function of the nanobubble size and applied compressive strain. The averaged field intensity of the nanobubbles refers to the averaged

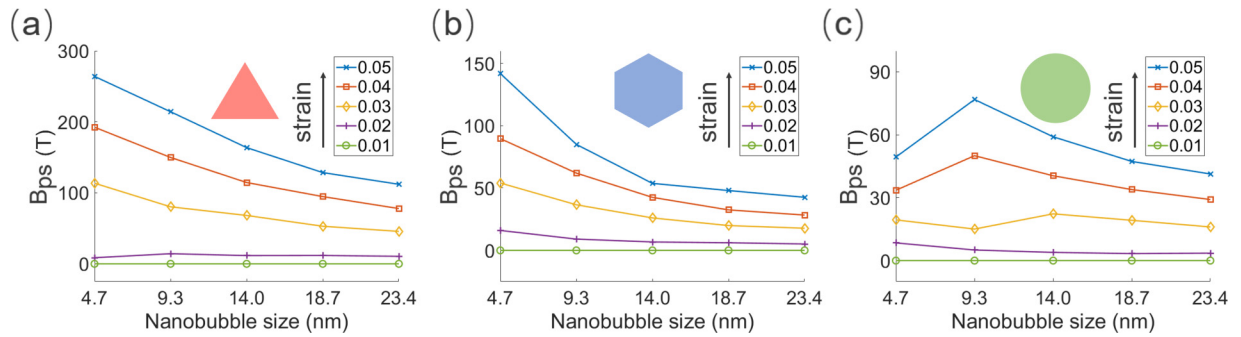


FIG. 5. The averaged intensity of pseudomagnetic field at interior regions of nanobubbles of three shapes as a function of the nanobubble size and applied compressive strain: (a) triangular, (b) hexagonal, and (c) circular. Data points on the same curve have the same compressive strain. In general, the intensity increases when the compressive strain increases or the nanobubble size decreases. Some exceptions found in the case of small circular nanobubbles are due to the transition of buckling morphology. See more discussions in main text.

absolute value of the field values at the interior region of the nanobubble since we are more interested in the field intensity away from the boundary. The largest circumscribed radius of the nanobubble is ~ 23.4 nm. For this size, the triangular nanobubble contains ~ 9000 atoms, the hexagonal nanobubble contains $\sim 18\,000$ atoms, and the circular nanobubble contains $\sim 22\,000$ atoms. In the subsequent discussion, the interior region of the nanobubble is quantitatively defined as the region where its closest distance to the nanobubble boundary is > 0.4 nm.

In the case of the triangular nanobubble, at small global compressive strain (i.e., 0.01 and 0.02), the field intensity is very low (~ 0 and 10 T, respectively) for all sizes [Fig. 5(a)]. However, as the global compressive strain increases to 0.03, the field intensities increase a lot due to the drastic increase in deflection (see Appendix C). At strain 0.03, the field intensities for all sizes are > 40 T. For the smallest bubble size (4.7 nm), the field intensity at strain 0.03 is already > 100 T, and the field intensity further increases to ~ 200 T at strain 0.04 [Fig. 5(a)]. Such sensitivity over applied compressive strain is observed for all nanobubble sizes.

On the other hand, at the same applied compressive strain, the larger the nanobubble size, the smaller the field intensity. The above trend is also observed in the case of the hexagonal bubble [Fig. 5(b)], although the field intensity is lower than that of the triangular nanobubble for the same nanobubble size and applied compressive strain. The field intensities in the case of the circular nanobubble are the lowest among all shapes [Fig. 5(c)]. However, different trends are observed for the effect of nanobubble sizes at large applied compressive strains, which are not observed for the other two shapes. For example, at strain 0.04 and 0.05, the field intensity for size 4.7 nm is lower than that for size 9.3 nm. The reason is that, for circular nanobubbles, when the bubble size increases, due to the constraint of the circular boundary, ripples appear (see Appendix C). Typically, the strain gradients at these ripples are very large and can lead to high field intensity compared with nonrippled bubble morphology, which explains the trend at strains beyond 0.04. Furthermore, we see that, at strain 0.03, the field intensity for size 9.3 nm is smaller than those of size 4.7 and 14.0 nm. This is because, for nonrippled bubble morphology (see Appendix C), large nanobubble size reduces the strain gradients at the same applied compressive strain.

B. Probe tip engineered pseudomagnetic fields

As mentioned in the introduction, the microscopy probe tip is frequently used to interact with the morphologies and strain patterns in two-dimensional materials [6,7,13,14]. In this section, we explore how the presence of the microscopy probe tip affects the intrinsic pseudomagnetic fields in buckled graphene structures. Particularly, we are interested in the sensitivity of the pseudomagnetic field against the tip-induced perturbation.

Figure 6(a) plots the original out-of-plane deflections (h) of three sizes of triangular nanobubbles. Figure 6(b) plots the tip-perturbed out-of-plane deflections ($h + \Delta h$) of triangular nanobubbles. Figure 6(c) plots the amount of change in out-of-plane deflection (Δh) for visual clarification. We can see that the heights of the nanobubbles increase due to the perturbation of the probe tip. The larger the nanobubble size, the larger increase in height. For the nanobubble of size 4.7 nm, the change in deflection is relatively uniform. This is because a tip whose diameter is comparable with the nanobubble size can almost affect the entire nanobubble. As the nanobubble size increases while keeping the tip size fixed, the change in out-of-plane deflection (Δh) of the nanobubble appears more localized under the tip. The change in deflection (Δh) in the center region of the nanobubble is significantly greater than that near the boundary, meaning that the tip mainly affects the area directly below it. Figure 6(d) shows the amount of relative change in out-of-plane deflection ($\Delta h/h$). It is found that the relative change in out-of-plane deflection for the nanobubble size of 4.7 nm appears rather uniform and is overall significantly larger than those of other bubble sizes. The above results show that a larger ratio of the tip size over the nanobubble size renders more global perturbation and higher relative change in local out-of-plane deflections.

The above sensitive change in deflections explains the high sensitivity of pseudomagnetic fields against tip-induced perturbation. Figure 6(e) plots the original pseudomagnetic field (B_{ps}) of triangular nanobubbles. Figure 6(f) plots the tip-perturbed pseudomagnetic field ($B_{ps} + \Delta B_{ps}$) of triangular nanobubbles, which still assume threefold symmetry. Figure 6(g) plots the amount of change in the pseudomagnetic field (ΔB_{ps}) for visual clarification, and Fig. 6(h) shows the amount of relative change in pseudomagnetic

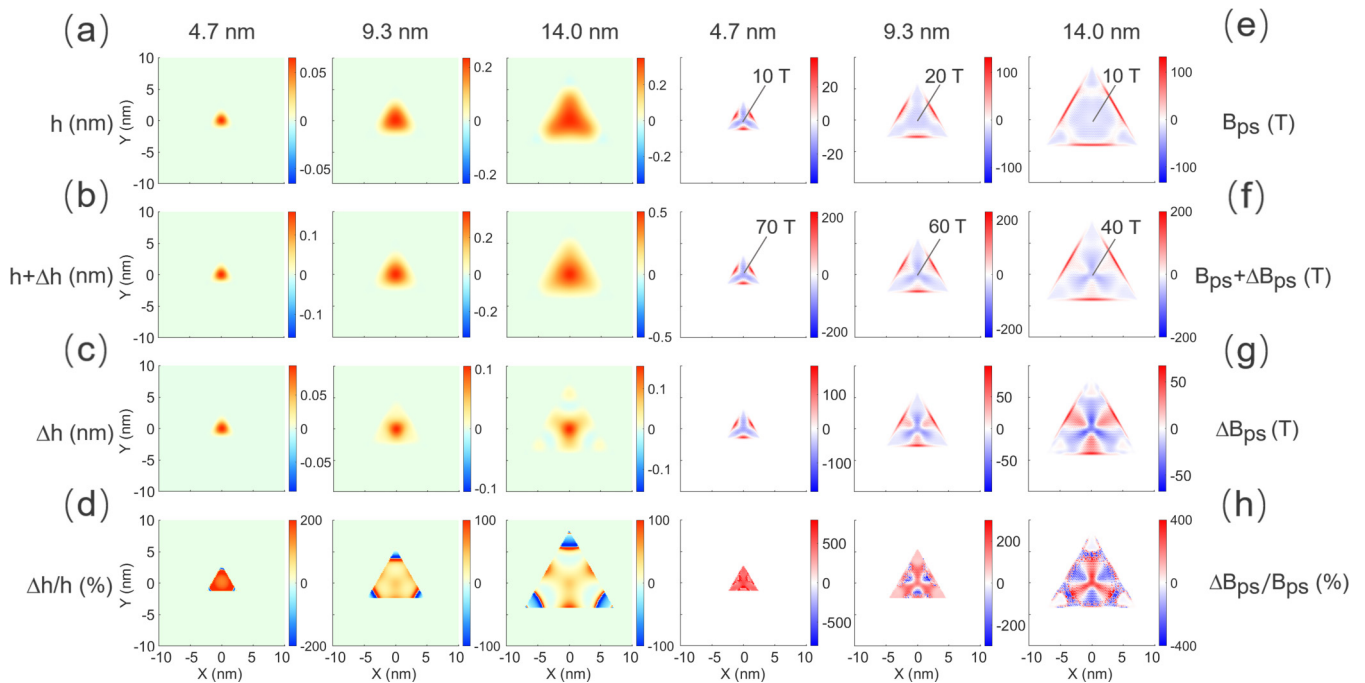


FIG. 6. The effect of microscopy probe tip on (a)–(d) the deflections and (e)–(h) pseudomagnetic fields in buckled graphene nanobubbles. Δh and ΔB_{ps} are tip-induced change in the out-of-plane deflection and pseudomagnetic field, respectively. Each column is labeled with corresponding nanobubble sizes (i.e., 4.7, 9.3, and 14.0 nm). The tip size is 2 nm, and the applied compressive strain is 0.02, for all cases. Larger ratio of tip size over nanobubble size renders stronger perturbation effects. Please note that, here, the field value of percentage increase is calculated on individual field point.

field ($\Delta B_{ps}/B_{ps}$). The distribution patterns of tip-perturbed pseudomagnetic fields are found to follow very much those of tip-perturbed deflections. The tip-perturbed pseudomagnetic fields can be a few times larger than their original values. A larger ratio of the tip size over the nanobubble size renders stronger perturbation effects.

Next, we investigate the effects of the probe tip size on several representative nanobubble models where the nanobubble size and globally applied compressive strain are fixed. Figure 7(a) shows the dependence of the maximum intensity of pseudomagnetic fields at the interior regions of three shapes of nanobubbles as a function of the probe tip size, where all nanobubbles have the same size (i.e., 9.3 nm) and the same applied compressive strain (i.e., 0.02). A threshold value of tip size (~ 5 nm) can be identified in these cases. For tip size smaller than the threshold value, the tip-perturbed pseudomagnetic field intensity increases drastically as the tip size increases. For tip size larger than the threshold value, the tip-perturbed pseudomagnetic field intensity increases with a much smaller rate as the tip size increases and gradually reaches a plateau. Figures 7(b) and 7(c) plot the amount of change and relative change due to the probe tip, respectively, where similar trends are observed.

Such a dependence on tip size can be interpreted as follows. For smaller tip sizes below the threshold value, the area of effect from the tip on the graphene nanobubble (i.e., the region where the carbon atoms can strongly feel the van der Waals force from the tip) expands as the tip size increases, which results in increased field intensity. As the tip size exceeds the threshold value, the area of effect from the tip covers the entire bubble. Because van der Waals forces decay rapidly

over long distances, the further increases in tip size could not significantly change the overall resultant force of the tip acting on the bubble, which explains the saturation trend. We also note that there is an unusual decrease in field intensity when the tip size increases from 4 to 5 nm. Based on the deformation profile, we find that, as the tip size approaches the threshold value, the energy-minimized tip-perturbed heights of nanobubbles have a sudden decrease [Fig. 7(d)], which in general could lead to decreased field intensity because the intensity of strain gradient is expected to decrease. Beyond the threshold value, the heights of nanobubbles start to slowly increase, in accordance with the saturation trend.

Furthermore, we investigate the effects of globally applied compressive strain on several representative nanobubble models where the nanobubble size and tip size are fixed. Figure 8(a) shows the resulting maximum pseudomagnetic field intensity at the interior regions of three different shapes of nanobubbles but with the same nanobubble size (i.e., 9.3 nm) and the same tip size (i.e., 2 nm). We find that the dependence of field intensity on the applied compressive strain can be divided into two regimes in these cases. When the strain is ~ 0 –0.015, the out-of-plane deflections for all nanobubbles without the tip are close to zero so that the intensities of the strain-induced pseudomagnetic field are zero (see Appendix D). Within such a strain range, as the strain increases, tip-perturbed pseudomagnetic field intensities also increase. The larger the strain, the larger the rate of increase in ΔB_{ps} [Fig. 8(b)]. However, such trends do not continue when the strain increases beyond 0.015, where we see that the rate of increase in ΔB_{ps} slows down as strain increases, and eventually ΔB_{ps} decreases. This is generally because larger

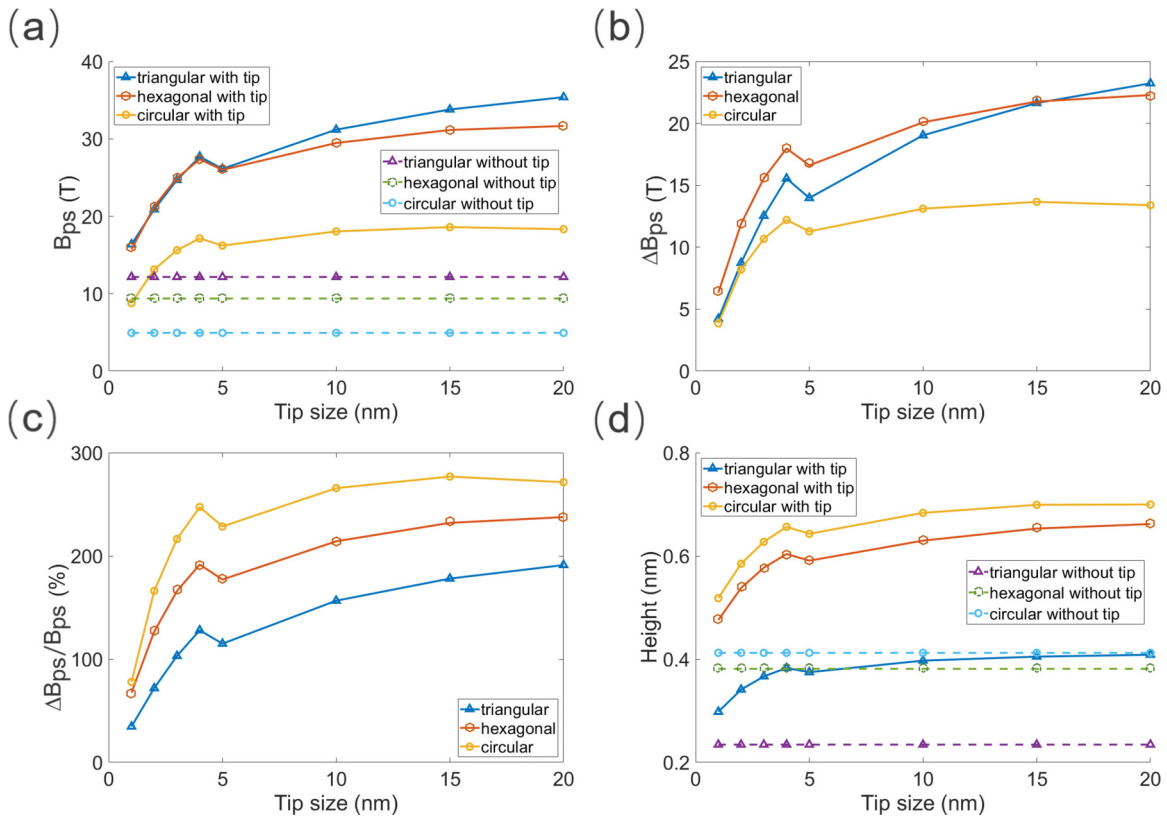


FIG. 7. Characterizations of pseudomagnetic fields at (a)–(c) the interior regions and (d) heights of nanobubbles of three shapes as a function of the probe tip size, where all nanobubbles have the same size (i.e., 9.3 nm) and the same applied compressive strain (i.e., 0.02). (a) Maximum field intensity at the interior region of nanobubbles. (b) The amount of increment due to the presence of tip. (c) The amount of relative change. The tip-perturbed effects tend to saturate as the tip size increases. See more discussions in main text.

compressive strain induces a buckled nanobubble, which is much stiffer and less flexible than its prebuckling flat state (i.e., the out-of-plane deflection close to zero), so that it is generally harder for the tip to induce strong local deformation; therefore, the enhancing effect from the tip reduces. However, exceptions may occur when the tip further induces new

buckled morphology. For the case of the circular nanobubble shown in Fig. 8(b), as the strain approaches 0.03, the ΔB_{ps} again increases. The reason is that (see Appendix D), at such strain, the tip can further induce the formation of ripples on the buckled nanobubble. The emergence of such ripples, which host large strain gradients, causes the increase in ΔB_{ps} .

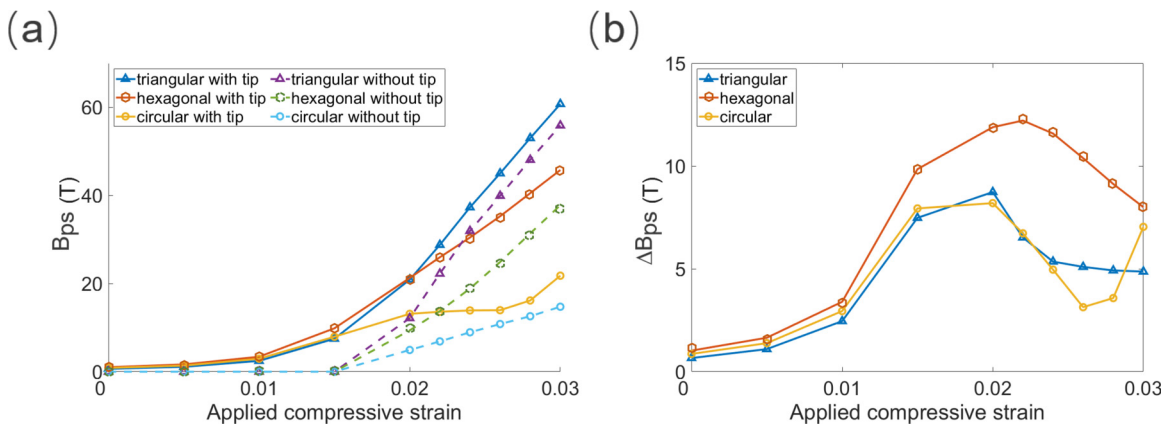


FIG. 8. Characterizations of pseudomagnetic fields at the interior regions of nanobubbles of three shapes as a function of applied compressive strain, where nanobubble size and tip size are all 9.3 and 2 nm, respectively. (a) Maximum field intensity at the interior region of nanobubbles. (b) The amount of increment due to the presence of tip. The probe tip can drastically increase field intensity below strain 0.015 because the original state of graphene is flat, and the tip can feasibly induce out-of-plane deflection. At larger strains, the trend in ΔB_{ps} appears complicated due to the buckled morphology. See more discussions in main text.

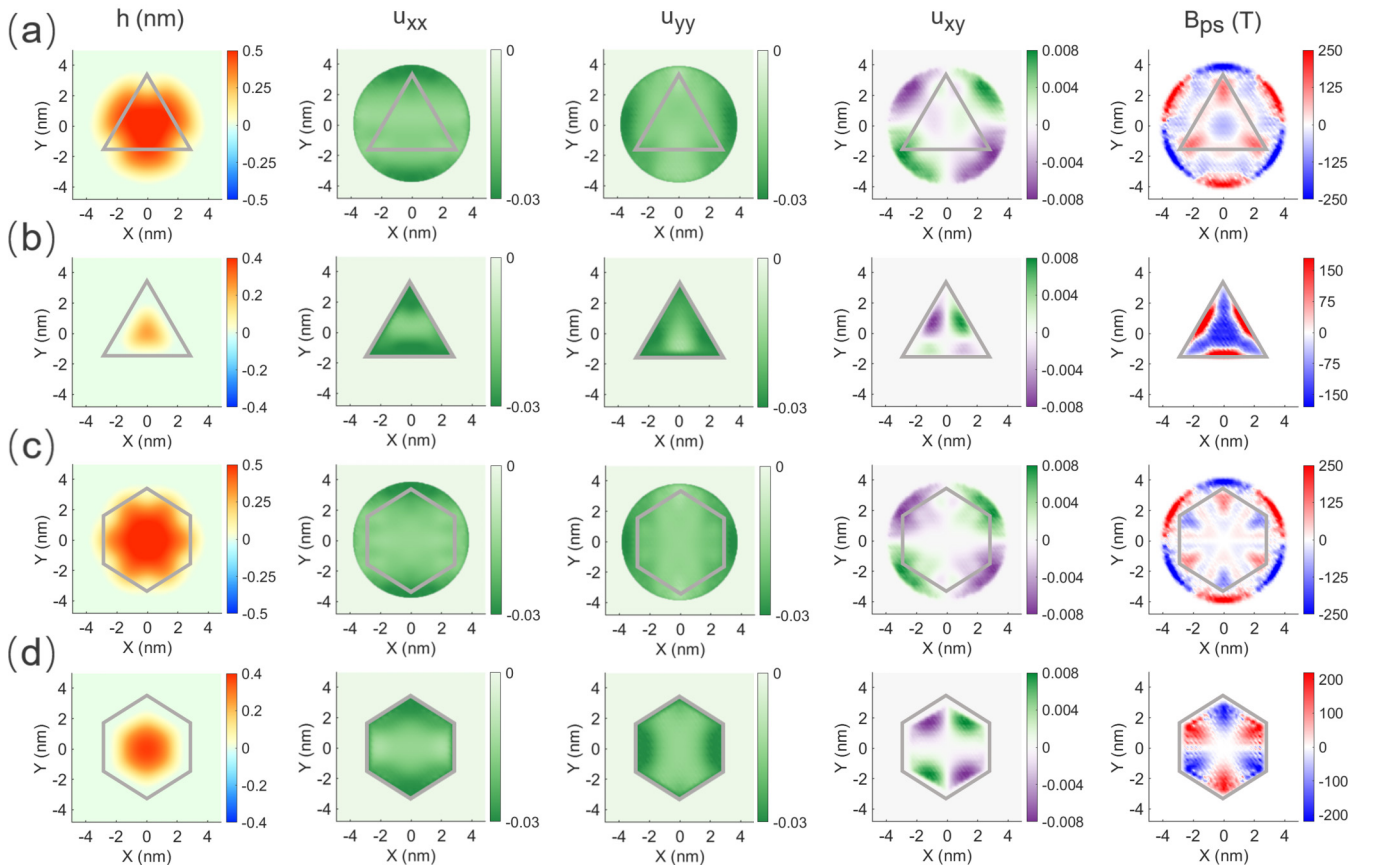


FIG. 9. Out-of-plane deflection (h), strain components (u_{xx} , u_{yy} , and u_{xy}), and the pseudomagnetic fields (B_{ps}) for triangular and hexagonal nanobubbles with fixed [i.e., (b) and (d)] and relaxed [i.e., (a) and (c)] boundaries. The gray lines represent original boundaries. For all cases, the nanobubble size and applied compressive strain are 4.7 nm and 0.03, respectively.

C. Effect of boundary relaxation

In the experiments, it might be difficult to fabricate a nanobubble with a strictly fixed preassigned boundary. To assess the effect of possible boundary relaxation in experiments, we also consider the relaxed boundary condition as described below. To assign relaxed boundaries in triangular nanobubbles, each atom at the vertex is subjected to a spring force to prevent it from moving far away from its initial position, with the spring constant taken as $0.1 \text{ eV}/\text{\AA}^2$ (see Appendix E for a discussion of the effect of the spring constant). In addition, a circular fixed boundary whose radius is 1 nm larger than the radius of the circumcircle of the triangular nanobubble is assigned so that atoms outside this additional circular boundary are not allowed to move. A similar assignment can be applied to the hexagonal nanobubbles. Since the relaxed circular nanobubble is largely analogous to the circular nanobubble of a larger fixed boundary, the following discussions mainly focus on the effect of the relaxed boundary condition of triangular and hexagonal nanobubbles.

Under the relaxed boundary condition, the out-of-plane buckled region expands beyond the original fixed boundary (see Appendix F). Because more atoms are allowed to move in the out-of-plane direction, the height of bubbles with relaxed boundaries in Fig. 9(a) is greater than bubbles with fixed boundaries in Fig. 9(b). The strain fields (u_{xx} , u_{yy} , and u_{xy}) also

differ from the case of fixed boundaries, while the symmetry remains. It can be further seen that the nanobubble with the fixed boundary condition in general has higher field intensity than the nanobubble with the relaxed boundary condition (note that the comparison is made on the region enclosed by the original boundary). This is because the relaxed boundary can generally reduce the magnitude of strain gradient within the area enclosed by the original fixed boundary. Furthermore, the distribution of pseudomagnetic fields inside the region enclosed by the original fixed boundary also has threefold symmetry, where a uniform pseudomagnetic field appears across the central region of the nanobubble in Fig. 9(a). In a word, the boundary relaxation generally preserves the rotational symmetry of pseudomagnetic fields and reduces their intensities. The above conclusion generally applies to the relaxed hexagonal boundary [Figs. 9(c) and 9(d)] as well, although more complicated distribution patterns of pseudomagnetic fields are found.

On a final note, in the case of the relaxed boundary, effects of the probe tip and the applied strain are expected to be largely consistent with the case of the fixed boundary because the relaxed boundary is qualitatively equivalent to a fixed boundary that encloses a larger area. For example (see Appendix F), the probe tip can enhance the field intensity of relaxed triangular bubbles, and the rate of enhancement reduces at larger applied strain.

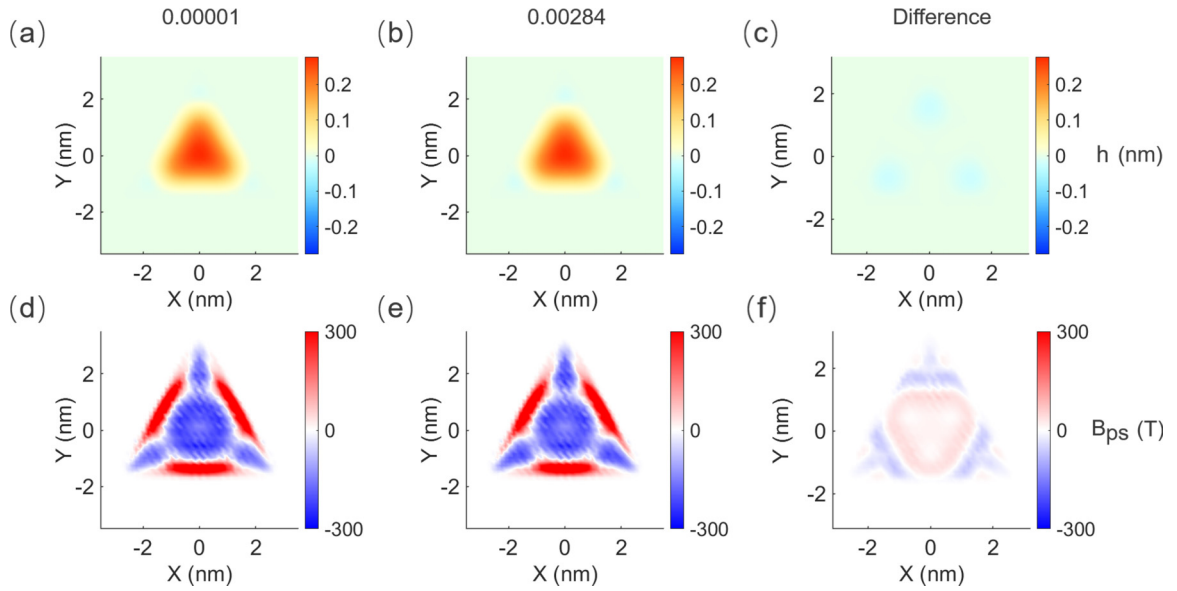


FIG. 10. Effect of the virtual substrate interaction on the out-of-plane deflections and pseudomagnetic fields of triangular nanobubbles. For all cases, the nanobubble size and applied strain are 4.7 nm and 0.035, respectively. (a) and (d) are results for $\epsilon = 0.00001$ eV, while (b) and (e) are results for $\epsilon = 0.00284$ eV [a much stronger interaction that mimics the van der Waals (vdW) interaction between graphene layers].

IV. SUMMARY

We systematically investigated the properties of compressive strain-induced pseudomagnetic fields in buckled graphene nanobubbles, which are the basic representative structures under compressive strains. Using MD simulations, we first validate our computational methods by explaining experimental observation [2] of a buckled triangular nanobubble possessing a pseudomagnetic field as high as 300 T. Then we investigate the effect of the nanobubble shape (triangular, hexagonal, and circular), the nanobubble size, applied compressive strain, and the presence of the microscopy probe tip (which is frequently used to interact with the morphologies and strain patterns). In general, we find that the pseudomagnetic field in buckled graphene nanobubbles is strong and highly sensitive to the applied compressive strain. A small increase in the applied strain may drastically increase the intensity of pseudomagnetic fields. In addition, coupled with the nanobubble size and the applied compressive strains, the presence of the probe tip can further induce significant local changes in the pseudomagnetic fields. Finally, we discuss the effect of the relaxed boundary which is closer to the actual experiment. In general, the field intensity is reduced due to boundary relaxation; nevertheless, its sensitivity against applied compressive strain and probe tip perturbation remains. Our work fills the gap of understanding on intensities and distribution patterns of the pseudomagnetic fields of buckled graphene nanobubbles with atomistic resolutions. These results may offer further guidance for designing electronic two-dimensional structures enabled by compressive strain engineering.

ACKNOWLEDGMENTS

This paper was supported by the National Natural Science Foundation of China (Grants No. 12272337 and No. 12002304), and the Distinguished Young Scientists

Fund from the Zhejiang Provincial Natural Science Foundation of China under Grant No. LR23A020001. The authors also acknowledge funding support from Zhejiang University.

APPENDIX A: EFFECT OF SUBSTRATE INTERACTION

Figure 10 shows the effect of the virtual substrate interaction on the out-of-plane deflections and pseudomagnetic fields of triangular nanobubbles. Although the value of epsilon has a huge increase, changes in the out-of-plane deflections

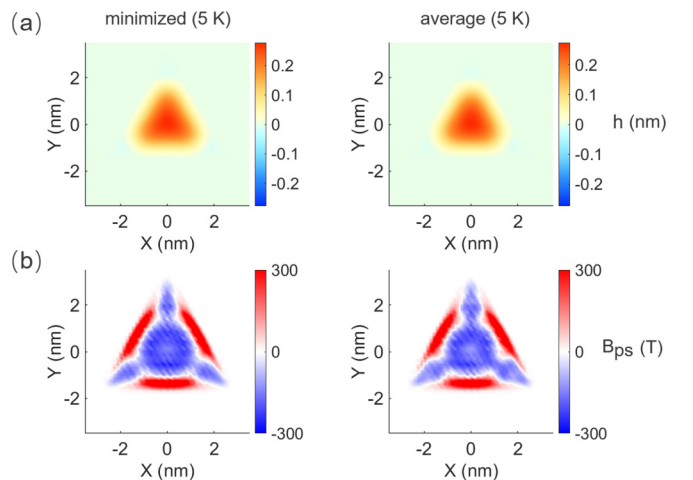


FIG. 11. Minimized (left column) and dynamic averaged (right column) (a) out-of-plane deflection and (b) pseudomagnetic field of triangular nanobubbles. For all cases, the nanobubble size, applied strain, and simulation temperature are 4.7 nm, 0.035, and 5 K respectively. The dynamic averaged field value is obtained by averaging the corresponding data for every 1 ps in a period of dynamics run of 50 ps under given temperature.

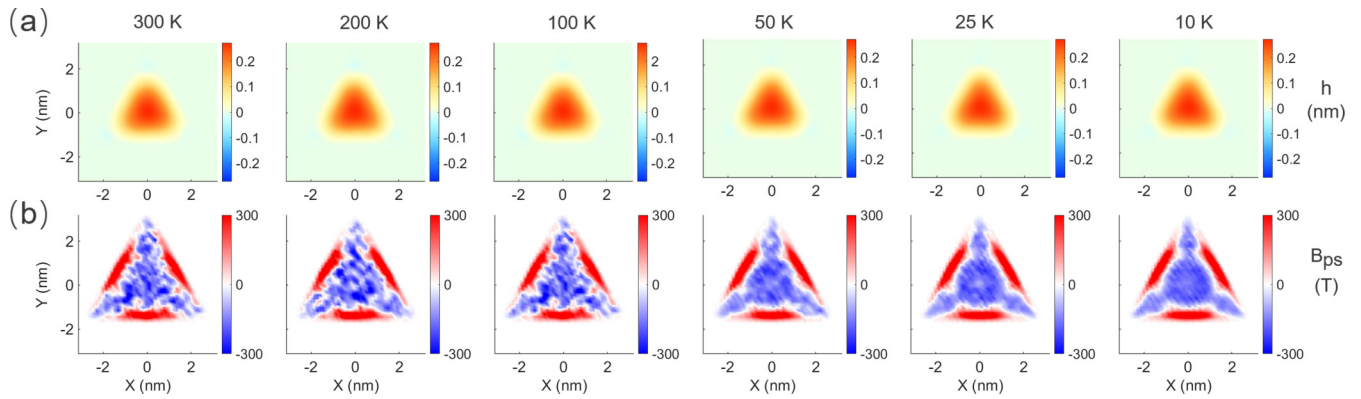


FIG. 12. Effects of the temperature on the dynamic averaged (a) out-of-plane deflection and (b) pseudomagnetic field of triangular nanobubbles. Each column is labeled with the simulated temperature. For all cases, the nanobubble size and applied strain are 4.7 nm and 0.035, respectively. See caption of Fig. 11 for the procedure of obtaining the dynamic averaged results.

and pseudomagnetic fields are focused on the region near the nanobubble boundary vertex. The influence is much smaller at the central region of the nanobubble. It is expected that stronger substrate interaction would effectively tighten the constraints from boundaries.

APPENDIX B: EFFECT OF TEMPERATURE

Figure 11 shows that the minimized and dynamic average results are similar. Figure 12 shows that when the temperature is high, the pseudomagnetic field becomes noisy and may be hard to measure experimentally. Therefore, it is necessary to lower the temperature. Note that the typical temperature for STM measurement is below 5 K. Here our computation suggests that as the temperature is reduced to about 10 K, the pseudomagnetic field approaches a stable state. In comparison with Fig. 11, the distributions and intensities of pseudomagnetic fields at 5 K and 10 K begin to look similar.

APPENDIX C: RIPPLE FORMATION AT LARGE STRAIN

Figure 13 shows the out-of-plane deflections at large strain for triangular nanobubbles, where apparent ripple formation is not observed. Figure 14 shows the ripple formation at large strain for circular nanobubbles.

APPENDIX D: EFFECT OF TIP ON NANOBUBBLE BUCKLING

Figure 15 shows the effect of tip for triangular nanobubbles. When the applied strain is less than 0.015, the out-plane deflection is very small so that the probe tip can cause a significant height variation. As the strain continues to increase, the effect of probe tip on the perturbation of nanobubble height diminishes, which means that the probe tip is no longer playing a major role. Figure 16 shows the effect of tip for circular nanobubbles. As the applied strain increases from 0.022 to 0.03, the surface of the circular nanobubble without probe tip remains ripple-free. After introducing the probe tip, ripples appear when the strain is increased to 0.028. The strain gradients and corresponding pseudomagnetic field intensities

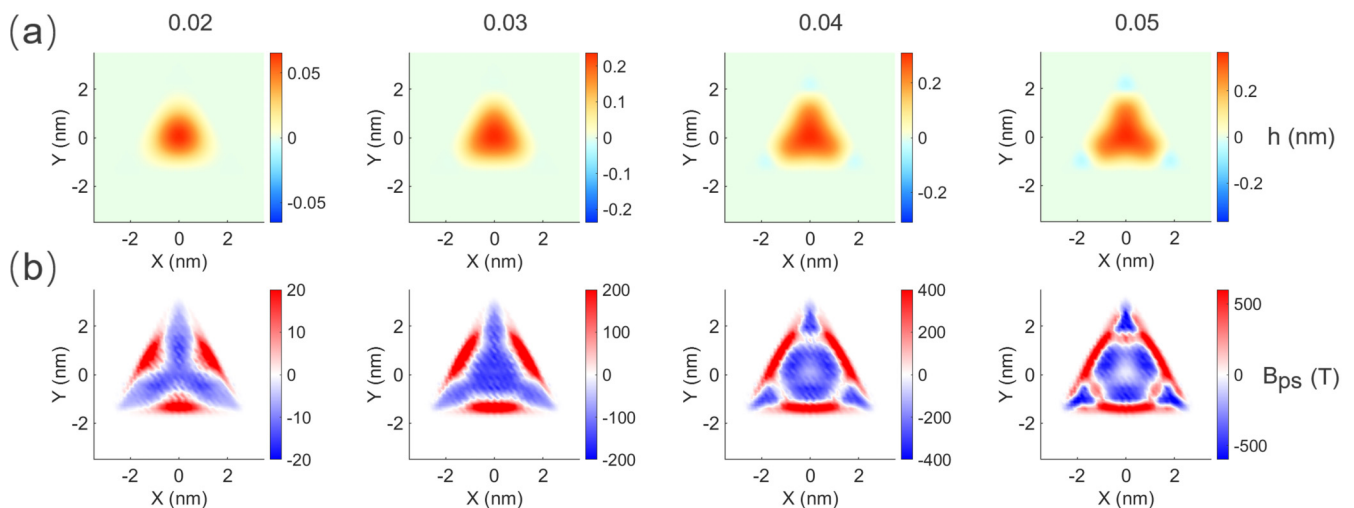


FIG. 13. (a) Out-of-plane deflections and (b) pseudomagnetic fields of triangular nanobubbles with different applied compressive strains. Each column is labeled with corresponding strains (i.e., 0.02, 0.03, 0.04, and 0.05). The nanobubble size is 4.7 nm in all cases.

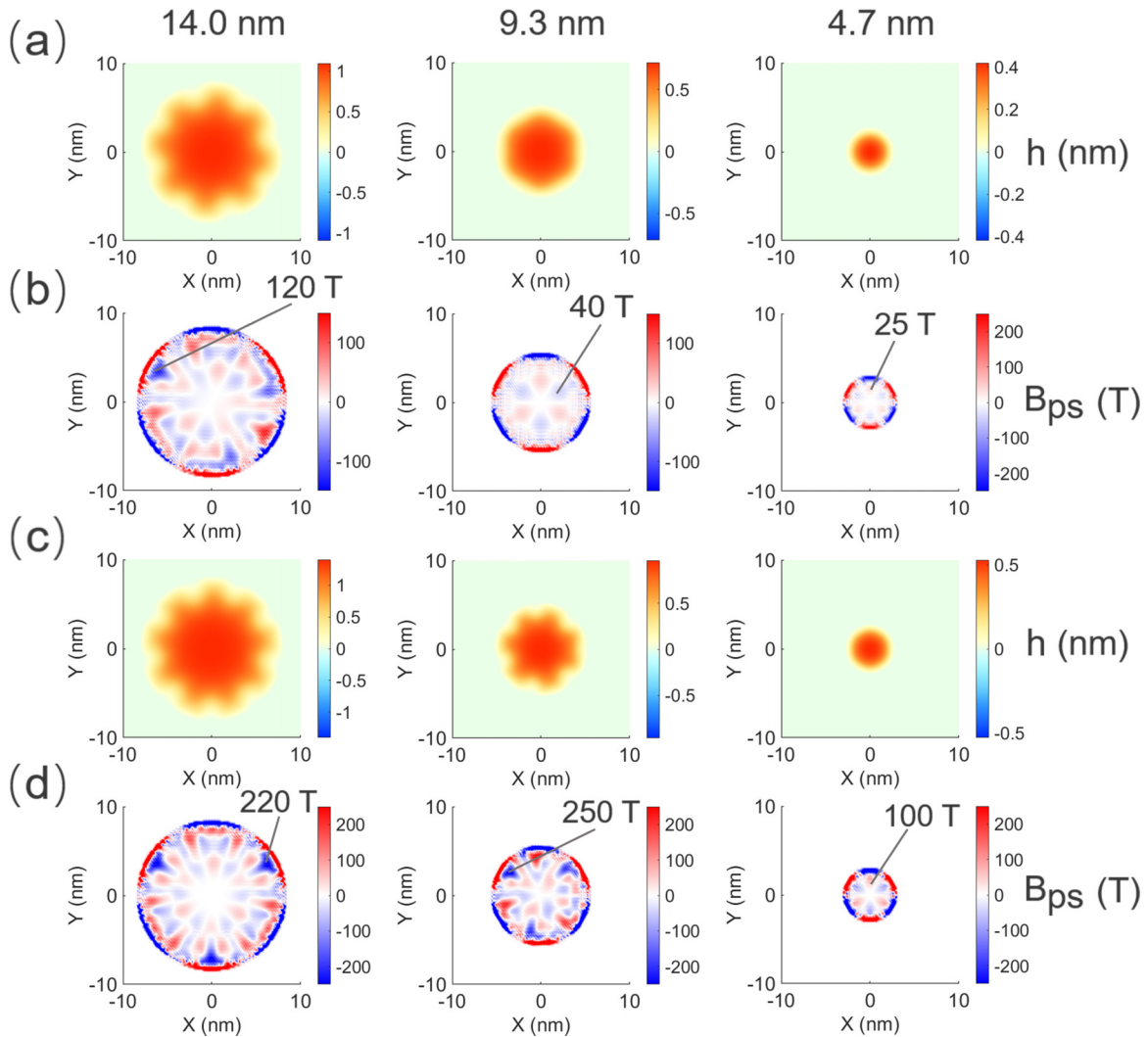


FIG. 14. Out-of-plane deflections [i.e., (a) and (c)] and pseudomagnetic fields [i.e., (b) and (d)] of circular nanobubbles. The applied compressive strain is 0.03 for (a) and (b). The applied compressive strain is 0.04 for (c) and (d). Each column is labeled with corresponding nanobubble sizes (i.e., 14.0, 9.3, and 4.7 nm).

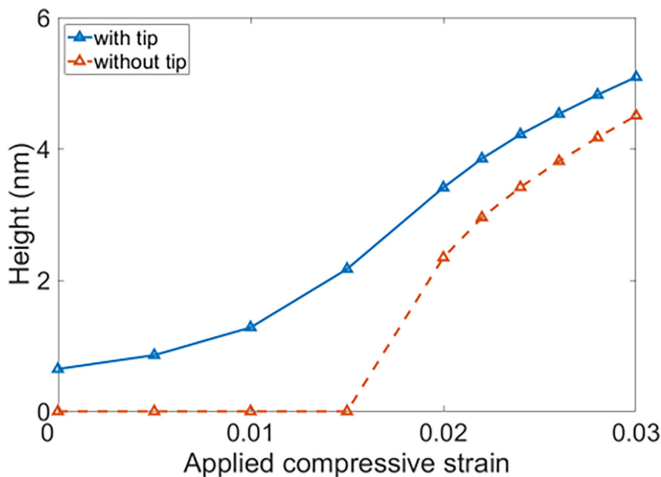


FIG. 15. The height of a nanobubble as a function of the applied compressive strain for triangular nanobubbles with and without the probe tip. For all data points, the nanobubble size and tip size are 9.3 and 2 nm, respectively.

are high at these ripples. The rippling effects are more significant when the applied strain is 0.03, which further enhances the field intensity. This is the source of the abnormal trend in Fig. 8(b).

APPENDIX E: EFFECT OF THE DEGREE OF BOUNDARY RELAXATION

Figure 17 shows the effect of the degree of boundary relaxation. The smaller the spring constant, the more relaxed the boundary so that the pseudomagnetic field intensity is slightly reduced at the interior region enclosed by the original fixed boundary. The distribution pattern changes in response to the different degree of relaxation.

APPENDIX F: TRIANGULAR NANOBUBBLES WITH RELAXED BOUNDARY

Figure 18 shows the additional changes in the in-plane displacements and out-of-plane deflection for triangular nanobubbles after the relaxed boundary condition is applied.

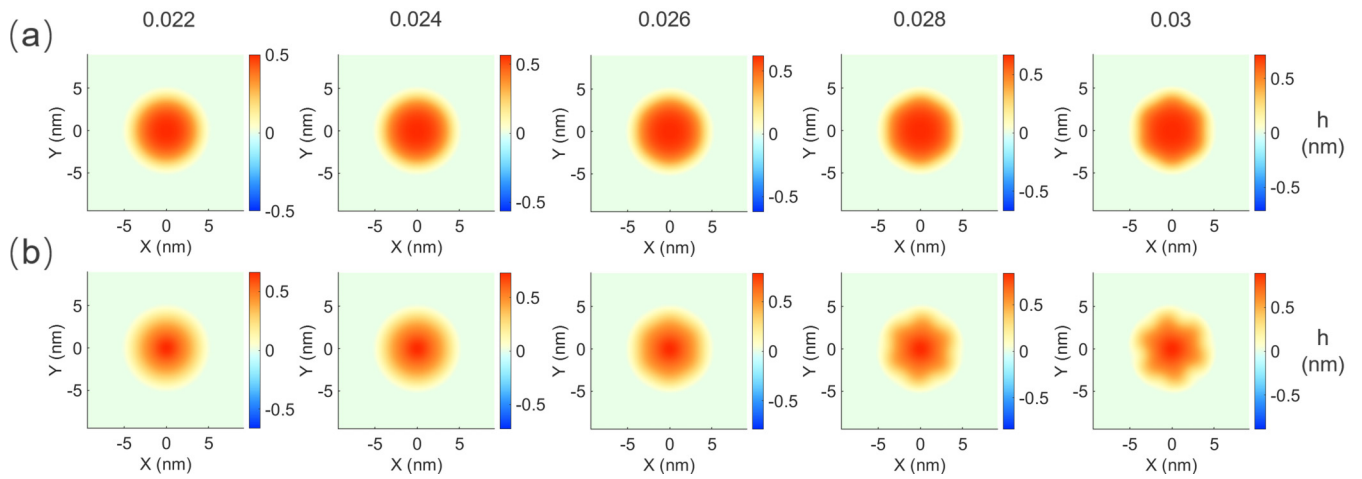


FIG. 16. The out-of-plane deflection of circular nanobubbles (a) without and (b) with the effect of probe tip. Each column is labeled with the corresponding applied compressive strain. For all cases, the nanobubble size and tip size are 9.3 and 2 nm, respectively.

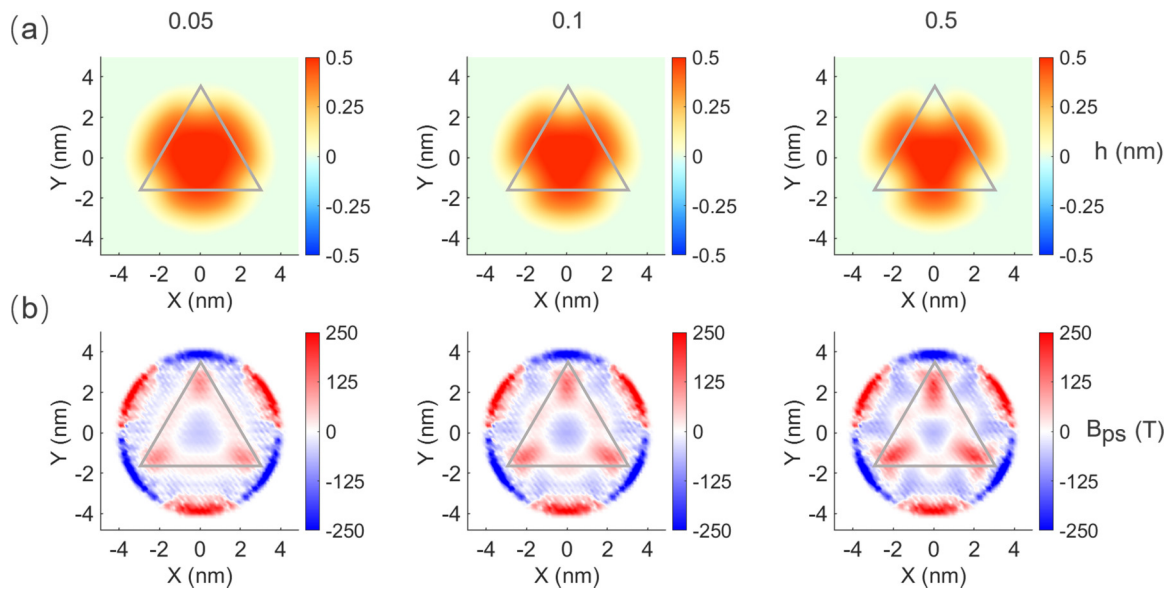


FIG. 17. (a) Out-of-plane deflection and (b) pseudomagnetic field of triangular relaxed nanobubbles with different degree of boundary relaxation. The gray lines represent original boundaries. Each column is labeled with the value of spring constant. The spring constant is used to characterize the degree of boundary relaxation. For all cases, the nanobubble size and applied strain are 4.7 nm and 0.035, respectively.

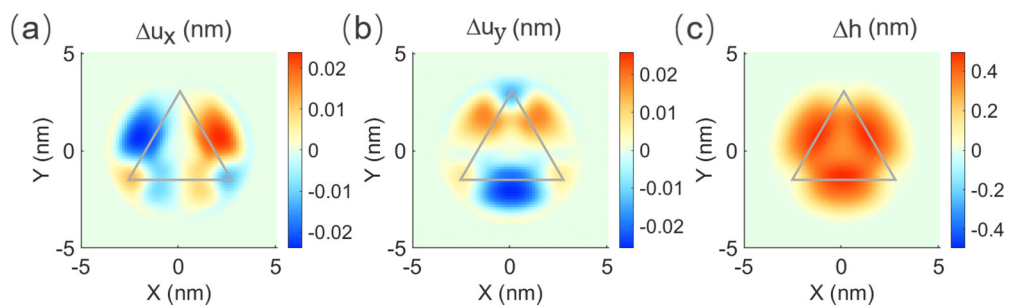


FIG. 18. Additional changes in the in-plane displacements (u_x , u_y) and out-of-plane deflection (h) for triangular nanobubbles after the relaxed boundary condition is applied. The gray lines represent original boundaries. The nanobubble size and applied compressive strain are 4.7 nm and 0.03, respectively.

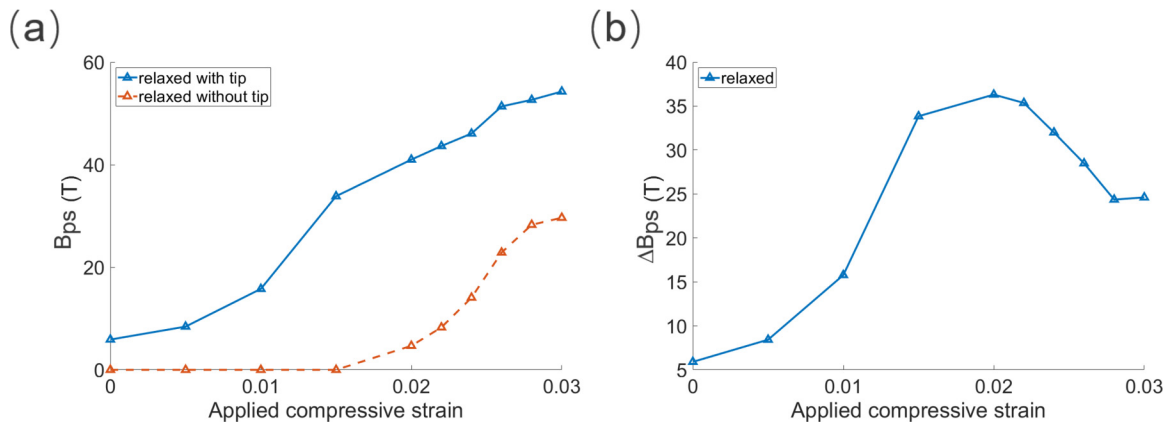


FIG. 19. Maximum intensity of pseudomagnetic field at the interior region enclosed by the original fixed boundary as a function of the applied compressive strain for triangular relaxed nanobubbles: (a) field intensity and (b) increment. The nanobubble size and tip size are fixed at 9.3 and 2 nm, respectively.

Figure 19 shows that for relaxed nanobubbles without the tip, when the strain is less than 0.015, the pseudomagnetic field intensities in nanobubbles are all close to zero. This means that there is basically no deformation in relaxed nanobubbles at this strain. Within such strain range, as the strain increases, the tip-perturbed intensity of pseudomagnetic field also increases. The larger the strain, the larger the increase in ΔB_{ps} [Fig. 19(b)]. However, such trend does not continue when the

strain increases beyond 0.015, where we see that the rate of increase in ΔB_{ps} reduces as strain increases, and eventually ΔB_{ps} decreases. This is similar to the explanation for the abnormal trend in Fig. 8. At larger compressive strain, the buckled nanobubble forms so that the entire nanobubble structure is more rigid so that the tip is generally harder to induce strong local deformation, therefore the enhancing effect from the tip reduces.

- [1] M. A. H. Vozmediano, M. I. Katsnelson, and F. Guinea, Gauge fields in graphene, *Phys. Rep.* **496**, 109 (2010).
- [2] N. Levy, S. A. Burke, K. L. Meaker, M. Panlasigui, A. Zettl, F. Guinea, A. H. C. Neto, and M. F. Crommie, Strain-induced pseudo-magnetic fields greater than 300 tesla in graphene nanobubbles, *Science* **329**, 544 (2010).
- [3] J. Mao, S. P. Milovanovic, M. Anđelković, X. Lai, Y. Cao, K. Watanabe, T. Taniguchi, L. Covaci, F. M. Peeters, A. K. Geim *et al.*, Evidence of flat bands and correlated states in buckled graphene superlattices, *Nature (London)* **584**, 215 (2020).
- [4] F. Guinea, M. I. Katsnelson, and A. K. Geim, Energy gaps and a zero-field quantum Hall effect in graphene by strain engineering, *Nat. Phys.* **6**, 30 (2010).
- [5] S. Zhu, J. A. Stroscio, and T. Li, Programmable Extreme Pseudomagnetic Fields in Graphene by a Uniaxial Stretch, *Phys. Rev. Lett.* **115**, 245501 (2015).
- [6] N. N. Klimov, S. Jung, S. Zhu, T. Li, C. A. Wright, S. D. Solares, D. B. Newell, N. B. Zhitenev, and J. A. Stroscio, Electromechanical properties of graphene drumheads, *Science* **336**, 1557 (2012).
- [7] P. Jia, W. Chen, J. Qiao, M. Zhang, X. Zheng, Z. Xue, R. Liang, C. Tian, L. He, Z. Di *et al.*, Programmable graphene nanobubbles with three-fold symmetric pseudo-magnetic fields, *Nat. Commun.* **10**, 3127 (2019).
- [8] Z. Qi, A. L. Kitt, H. S. Park, V. M. Pereira, D. K. Campbell, and A. H. Castro Neto, Pseudomagnetic fields in graphene nanobubbles of constrained geometry: A molecular dynamics study, *Phys. Rev. B* **90**, 125419 (2014).
- [9] S. P. Milovanović, M. Anđelković, L. Covaci, and F. M. Peeters, Band flattening in buckled monolayer graphene, *Phys. Rev. B* **102**, 245427 (2020).
- [10] S. Plimpton, Fast parallel algorithms for short-range molecular dynamics, *J. Comput. Phys.* **117**, 1 (1995).
- [11] A. Castellanos-Gomez, R. Roldán, E. Cappelluti, M. Buscema, F. Guinea, H. S. J. van der Zant, and G. A. Steele, Local strain engineering in atomically thin MoS₂, *Nano Lett.* **13**, 5361 (2013).
- [12] S. Lou, Y. Liu, F. Yang, S. Lin, R. Zhang, Y. Deng, M. Wang, K. B. Tom, F. Zhou, H. Ding *et al.*, Three-dimensional architecture enabled by strained two-dimensional material heterojunction, *Nano Lett.* **18**, 1819 (2018).
- [13] S. Manzeli, A. Allain, A. Ghadimi, and A. Kis, Piezoresistivity and strain-induced band gap tuning in atomically thin MoS₂, *Nano Lett.* **15**, 5330 (2015).
- [14] S. Bertolazzi, J. Brivio, and A. Kis, Stretching and breaking of ultrathin MoS₂, *ACS Nano* **5**, 9703 (2011).
- [15] S. Zhu, Y. Huang, N. N. Klimov, D. B. Newell, N. B. Zhitenev, J. A. Stroscio, S. D. Solares, and T. Li, Pseudomagnetic fields in a locally strained graphene drumhead, *Phys. Rev. B* **90**, 075426 (2014).
- [16] S. J. Stuart, A. B. Tutein, and J. A. Harrison, A reactive potential for hydrocarbons with intermolecular interactions, *J. Chem. Phys.* **112**, 6472 (2000).
- [17] A. K. Rappe, C. J. Casewit, K. S. Colwell, W. A. Goddard, and W. M. Skiff, UFF, a full periodic table force field for molecular

- mechanics and molecular dynamics simulations, *J. Am. Chem. Soc.* **114**, 10024 (1992).
- [18] A. H. Castro Neto, F. Guinea, N. M. R. Peres, K. S. Novoselov, and A. K. Geim, The electronic properties of graphene, *Rev. Mod. Phys.* **81**, 109 (2009).
- [19] K.-J. Kim, Ya. M. Blanter, and K.-H. Ahn, Interplay between real and pseudomagnetic field in graphene with strain, *Phys. Rev. B* **84**, 081401(R) (2011).
- [20] H. S. Seung and D. R. Nelson, Defects in flexible membranes with crystalline order, *Phys. Rev. A* **38**, 1005 (1988).